Sea surface winds from sun glitter observations

Lucien Wald, Jean-Marie Monget

JOURNAL OF GEOPHYSICAL RESEARCH, VOL. 88, NO. C4, PAGES 2547–2555, MARCH 20, 1983

Sea Surface Winds From Sun Glitter Observations

L. WALD AND J. M. MONGET

Centre de Télédétection et d'Analyse des Milieux Naturels, Ecole Nationale Supérieure des Mines de Paris 06565 Valbonne cedex, France

Solar light reflected by the surface of the sea depends strongly on the sea state which is driven by the wind. The relationship between the reflected light and wind speed is described by the well-known model of Cox and Munk. Using their model, a method is derived for the retrieval of the synoptic field of wind magnitude from measurements of the glitter pattern from space. This method is applied to data obtained by the TIROS-N satellite series. Comparison of the wind estimated in this way and the wind derived from isobaric charts shows very close agreement. The method is simple and has application over broad geographical areas.

1. INTRODUCTION

The pattern of dancing highlights caused by the reflection of the sun from a water surface is called the sun glitter pattern. The investigations to date have established the relationships among glitter pattern characteristics, surface roughness, and near-surface wind speed, and have demonstrated the feasibility of making useful measurements from spacecraft [*Soules*, 1970; *McClain and Strong*, 1969; *Strong and Ruff*, 1970; *Webber*, 1971; *Levanon*, 1971; *Plass et al.*, 1977; *Wylie et al.*, 1981; *Rozenberg and Mullamaa*, 1965; *LaViolette et al.*, 1980].

It is well known that the surface of the ocean may be differentiated into small, mirrorlike facets that have individual characteristic slopes, each of which reflects according to the law of reflection. At spacecraft altitude, the reflecting facets will not be individually resolved. Therefore the apparent radiance of the sea surface in any direction will depend on the fraction of the area having the proper slope for specular reflection. The observed pattern shows a radiance decreasing smoothly outward from its center, since greater and therefore less frequent slopes are required as the distance from the center increases. As the surface roughness increases with sea state, the pattern broadens and the level of radiance at the center decreases. Thus either a measurement of the absolute radiance of the center of the glitter pattern or some suitable measurements of the pattern size will give an indication of the sea state and of the wind speed as well, since the broadening of the pattern is caused primarily by the capillary waves which are very sensitive to the local wind.

This paper presents a very simple method to retrieve wind speed from measurements of the broadening of the glitter pattern sensed by satellite. This method originated with an idea of *Rozenberg and Mullamaa* [1965], developed by *Webber* [1971], using the wave slope–frequency distribution model of *Cox and Munk* [1954].

It is then applied to sun glint images obtained by the advanced very high resolution radiometer (AVHRR) sensor aboard the TIROS-N satellite series. The wind speeds and directions computed from the glitter pattern are finally compared to those measured from meteorological isobaric charts.

2. THE WAVE SLOPES' STATISTICAL DISTRIBUTION

The frequency distribution of the occurrence of wave slopes was studied by *Cox and Munk* [1954] for a fully developed sea as a function of the wind speed, near the island of Maui (Hawaii) with wind speeds up to 14 m/s. They found that this distribution can be fitted, to a first approximation, by a two-dimensional Gaussian distribution:

$$p(Z_{x1}Z_y) = \frac{1}{2\pi\sigma_c\sigma_u} \exp\left\{-\frac{1}{2}\left[\left(\frac{Z_x}{\sigma_c}\right)^2 + \left(\frac{Z_y}{\sigma_u}\right)^2\right]\right\} \quad (1)$$

where Z_x and Z_y are the slope components crosswind and upwind, respectively, and σ_c and σ_u are the corresponding rms values of the slope components; ${\sigma_c}^2$ and ${\sigma_u}^2$ are linearly related to the wind speed V:

$$\begin{aligned} {\sigma_c}^2 &= 0.003 + 0.00192V \\ {\sigma_u}^2 &= 0.000 + 0.00316V \\ \sigma^2 &= {\sigma_u}^2 + {\sigma_c}^2 = 0.003 + 0.00512V \end{aligned} \quad (2)$$

where V is given in meters per second.

These authors also observe that σ^2 is independent of variations in wind direction and thus its use gives a better determination of wind speed than either ${\sigma_u}^2$ or ${\sigma_c}^2$ separately. Therefore we assume the distribution of the occurrence of wave slopes to be isotropic for the determination of wind speed. The wind direction is determined independently, by identifying the direction of the glitter pattern ellipse. Any errors in the determination of the direction of the major axis of the ellipse, and thus in the identification of the wind direction, do not affect the wind speed measurement.

According to Figure 1, θ and ϕ are the observer zenith and azimuthal angles, respectively, and θ_0 and ϕ_0 are the sun zenith and azimuthal angles. The probability for seeing glitter in direction (θ, ϕ) when the sun is in direction (θ_0, ϕ_0) is

$$\begin{aligned} p(\theta, \phi; \theta_0, \phi_0; V) &= \frac{1}{\pi\sigma^2} \exp\left(-\frac{\tan^2\theta_n}{\sigma^2}\right) \\ &= P(\theta_n, V) \end{aligned} \quad (3)$$

with

$${Z_x}^2 + {Z_y}^2 = \tan^2\theta_n \quad (4)$$

where (θ_n, ϕ_n) are the components of the normal vector to the slope for which the specular reflection conditions are fulfilled (Figure 1).

With ω as the reflection angle, θ_n can be deduced from the following equations [*Viollier et al.*, 1980]:

$$\cos 2\omega = \cos\theta\cos\theta_0 + \sin\theta\sin\theta_0\cos(\phi - \phi_0) \quad (5)$$

$$\theta_n = \arccos\left(\frac{\cos\theta + \cos\theta_0}{2\cos\omega}\right) \quad (6)$$

Paper number 2C1787.
0148-0227/83/002C-1787$05.00

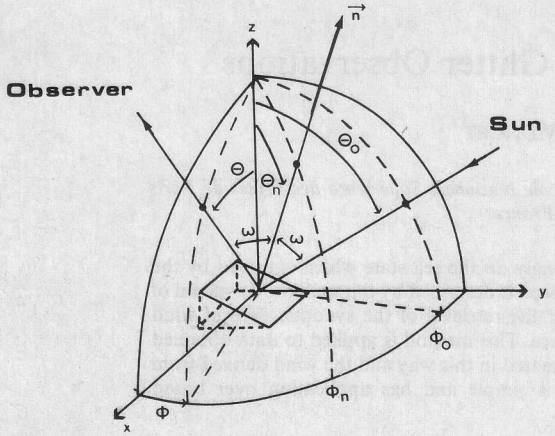

Fig. 1. Reflection geometry. The solar radiation reflects against the wave slope defined by the normal vector **n**. The reflected radiation is observed in the (θ, ϕ) direction.

In the absence of atmosphere, the glitter radiance $L_g(\theta, \phi; \theta_0, \phi_0; V)$ is a function of the probability density:

$$L_g(\theta, \phi; \theta_0, \phi_0; V) = \frac{E_0 r(\omega) P(\theta_n, V)}{4 \cos\theta \cos^4\theta_n} \tag{7}$$

where E_0 is the spectral solar irradiance at the top of the atmosphere and $r(\omega)$ is the reflection factor computed for a perfectly smooth surface (Fresnel reflection factor).

When normalized by the incident irradiance, this equation becomes

$$R_g(\theta, \phi; \theta_0, \phi_0; V) = \frac{\pi r(\omega) P(\theta_n, V)}{4 \cos\theta_0 \cos\theta \cos^4\theta_n} \tag{8}$$

where R_g is called the glitter reflectance.

From this equation, three methods can be derived to infer surface winds from sun glint observations. The first one deals with absolute value of glitter reflectance after the other sources of radiation have been removed, while the other two methods rely on the geometrical characteristics of the sensed glitter pattern rather than on the brightness values. The second one is based upon the shifting of the brightest point away from its geometrical location for null wind, while the third method measures the broadening of the pattern as the sea roughens. These methods are detailed in the following sections.

3. Absolute Determination of Sun Glitter Reflectance

In addition to the sun glitter, other sources of radiation have to be considered in spacecraft observations: (1) the skylight and sunlight scattered by particles beneath the sea surface, (2) the skylight reflected at the sea surface, and (3) the scattered light in the air column, separating the sensor from the water.

These sources affect the determination of the sun glitter reflectance. Each term will be discussed, and it will be shown that if some terms are negligible, the accurate estimation of the remaining contribution can hardly be achieved and this renders the absolute determination of sun glitter reflectance very difficult.

The influence of the first source can be easily minimized using a spectral band centered around 1 μm. At this wavelength, the absorption coefficient is very large [*Jerlov*, 1976], and consequently no radiation is backscattered from the interior of the sea, except in some coastal areas where the top layer backscattering volume is thick.

Then the reflectance R measured from space can be written [*Wald and Monget*, 1982]:

$$R = R_A + T(R_g + R_{sky}) \tag{9}$$

where R_A is the reflectance backscattered by the atmosphere, T is the atmospheric transmittance, and R_g and R_{sky} are the sunlight and skylight reflected at the sea surface.

The albedo of sea under diffuse skylight depends on the spatial distribution of radiance from the sky dome and on the sea state. It ranges from 10% for a smooth sea and a clear sky to 4% for a rough sea and an overcast sky [*Cox and Munk*, 1955]. On the other hand, the sky downwelling flux varies with direct sunlight, and its relative importance compared with the direct flux increases when the sun zenith angle increases. According to *Ivanoff* [1975] and *Plass et al.* [1975], for the wavelength concerned, the reflectance due to the reflected skylight can reach 5% for sun zenith angles greater than 70°, but becomes negligible for lower angles. We therefore conclude that the effect of reflected skylight can be neglected for the sun zenith angles under concern.

The atmospheric backscatter term R_A mainly consists of Mie scattering due to particulates. Rayleigh (molecular) scattering is negligible. *Viollier et al.* [1980] have shown that, for such wavelengths, R_A is only slightly modified (a few tenths) when specular reflection is taken into account. To a first approximation, R_A can be considered as a constant background noise of the order of 1%. Thus there are two important variables, T and R_A, which are necessary to convert the reflectance measured from space into sun glint reflectance. Accurate results require additional information such as the spectral extinction coefficient.

Furthermore, when the sea roughens, foam appears and increases the reflection factor. Recently, *Monahan and Muircheartaigh* [1980] underlined the complexity of description of oceanic whitecap coverage dependence on wind speed. They point out that any factor altering the mean lifetimes of whitecaps, such as thermal stability of the lower atmosphere and water temperature, will affect oceanic whitecap coverage. *Ross and Cardone* [1974] showed that white water formation by mechanical tearing away of wave crests with the resultant formation of spume lines becomes important at wind speeds above 9 m/s. Considering these effects, the foam can be modeled to a first approximation by patches of Lambertian nondispersive reflectors, each of which has a reflection factor of f. The global reflection factor r' is thus composed of a Lambertian and a non-Lambertian part [*Wald and Monget*, 1982]:

$$r'(\omega, V) = fs(V) + [1 - s(V)]r(\omega) \tag{10}$$

where $s(V)$ is the fraction of the sea covered by foam.

Values of s versus the wind speed can be found in the works by *Ross et al.* [1970], *Ross and Cardone* [1974], and *Monahan and Muircheartaigh* [1980]. For moderate wind speeds, the foam patches are nearly parallel to the wave slopes, and one can assume that the frequency distribution of the occurrence of foam slopes is the same as the distribution of the wave slopes. Then $r(\omega)$ is replaced by $r'(\omega, V)$ in (8), which can be solved numerically for V. But for higher wind speeds the distribution of the slopes of the foam patches is no longer the same as that for the wave slopes. From evidence this distribution will greatly affect the wind speed estimated from sun glint reflectance, but it does not seem to have been investigated, and no result for it was found in the literature by the authors.

It must be added that research on foam optical properties is

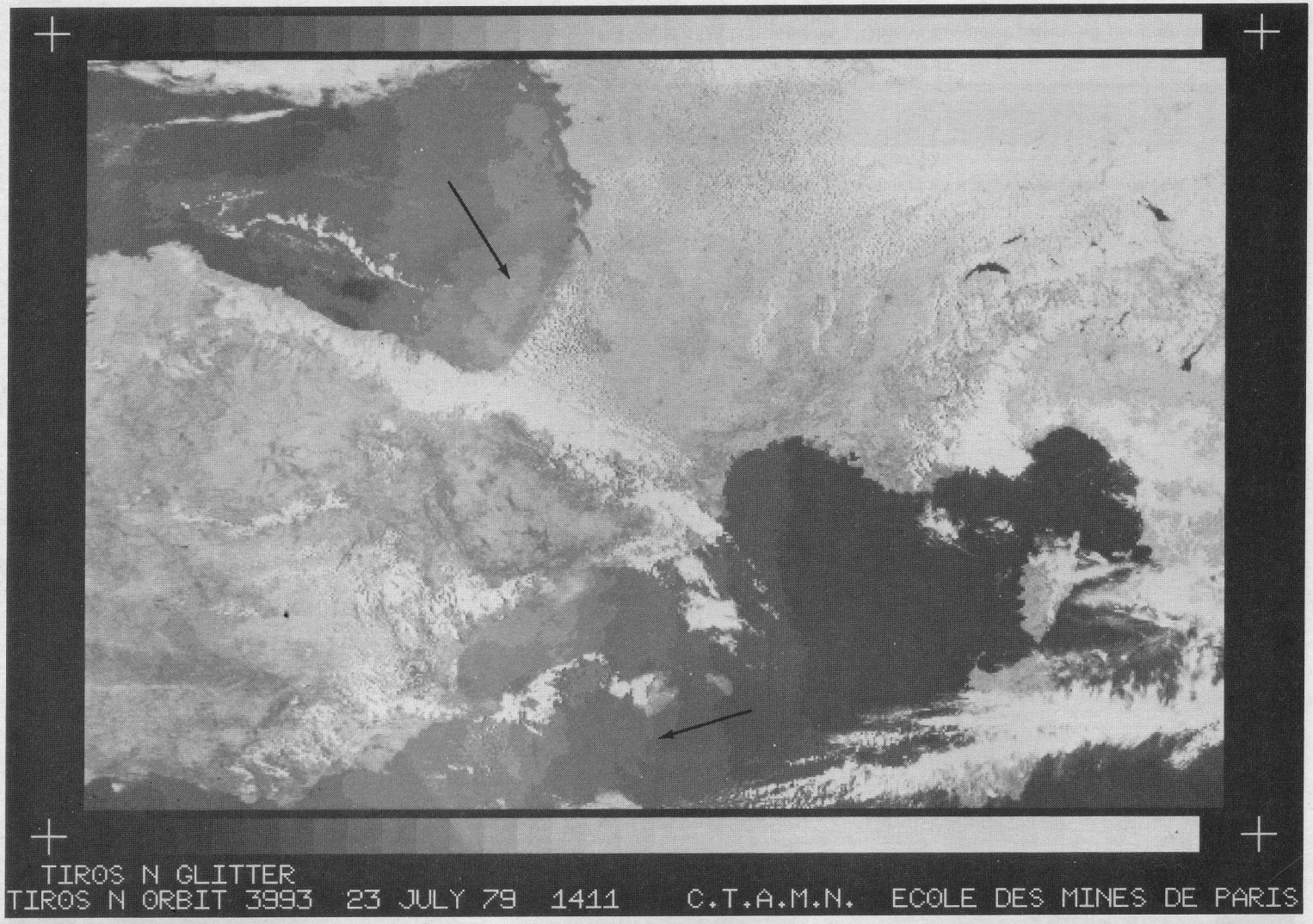

Fig. 2. TIROS-N AVHRR (channel 2) imagery taken on July 23, 1979, at 1410 UT, orbit 3993. Two glitter patterns are visible, one in the Bay of Biscay and the other near the Mediterranean Spanish coast. Arrows indicate the direction of the wind.

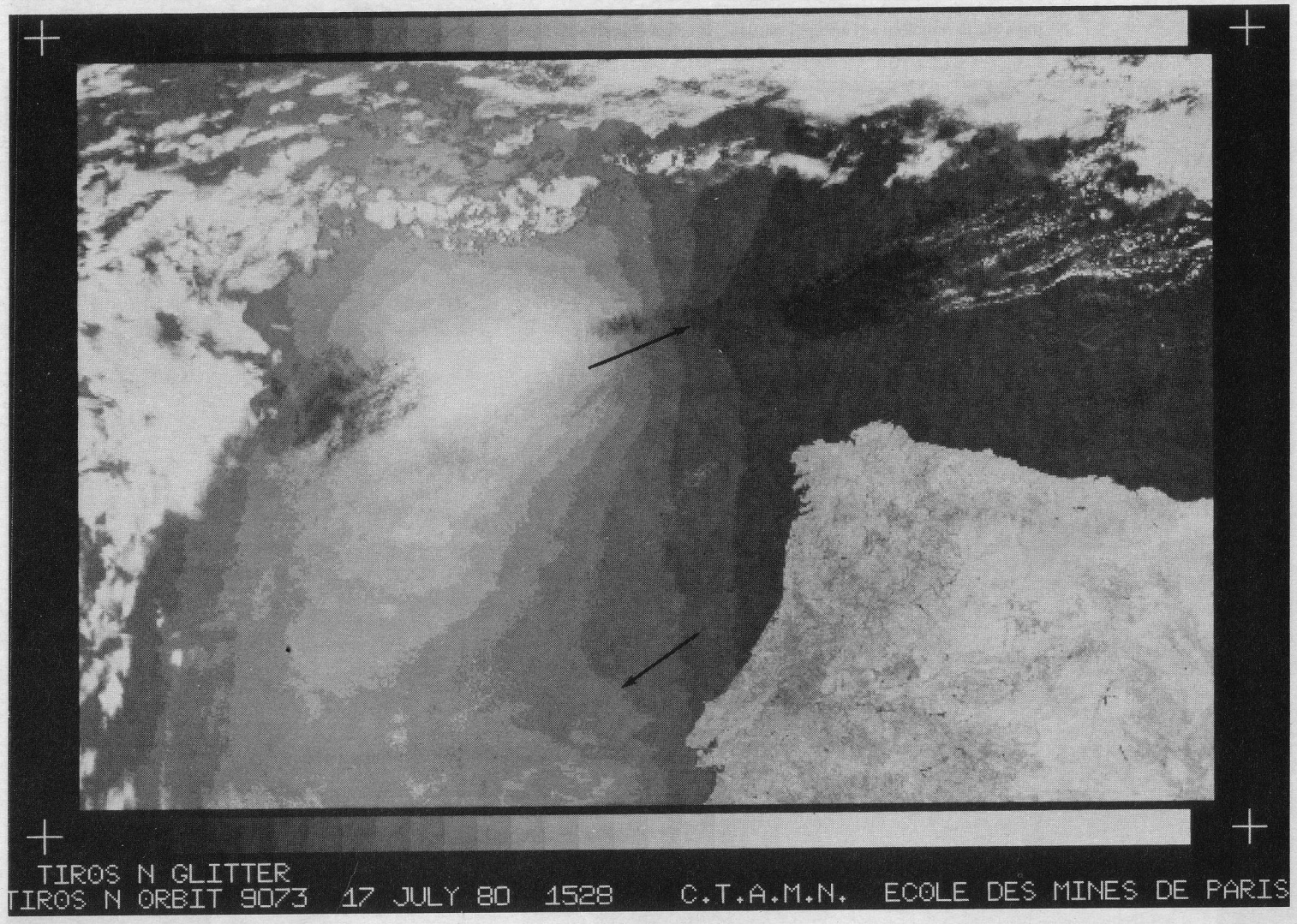

Fig. 3. TIROS-N AVHRR (channel 2) imagery taken on July, 17, 1980, at 1528 UT, orbit 9073. Observe the glitter pattern off the Portugal coast. Arrows indicate the direction of the wind.

sorely needed. The spectral albedo of the foam was arbitrarily set to 0.45 by *Quenzel and Kaestner* [1980] and to 0.9 by *Gordon and Jacobs* [1977]. These rough assumptions involve very great uncertainty of the order of 100% in the determination of the global reflection factor r'.

It follows from the previous discussion that accurate estimations of the absolute value of R_g are difficult to obtain and that the major drawback of this first described method is its complexity since other sources of radiation and foam coverage must be known exactly. However, in some cases where R_{sky} and the foam were negligible, *Wylie et al.* [1981] demonstrated a close agreement (± 0.5 m/s) between the winds computed from estimations of R_g and those from buoy anemometer measurements.

4. Wind Speed and Glitter Pattern Characteristics

The second method relies on one of the main results of *Cox and Munk* [1954]. They observed that the mean square slope, regardless of direction, increases linearly with wind speed, reaching a value of $(\tan^2 16°)$ for a wind speed of 14 m/s. This increase of the mean square slope implies the shifting of the glitter pattern toward the horizon; it was also clearly demonstrated by *Plass et al.* [1977]. Thus the wind speed can be inferred from measurement of the displacement of the brightest point away from its theoretical position for null wind, whatever the brightness.

However, this method requires (1) very precise knowledge of the geographical locations of the points of the field observed from space and (2) exact determination of the brightest point. Hence this method is rather complicated and cannot be of wide use.

The third method we present generalizes the work of *Webber* [1971], whose theoretical paper, after an idea of *Rozenberg and Mullamaa* [1965], explained how to use a substantial portion of the glitter pattern image in order to relate relative radiance measurements within the pattern to the Cox and Munk statistics. It is based on the determination of the distance from the pattern center of one or more isoradiance contours measured in relation to the center radiance. In the generalized method, the center of the pattern does not play any particular role, and wind speed can be inferred on purely geometric grounds by the measurement of the distance between two arbitrary isophotes.

The influence of the atmosphere is first eliminated using a straightforward algorithm based on the determination of relative measurements (rescaling) followed by ratioing.

If R_A is assumed to be spatially constant, it can be estimated by measurements taken away from the glitter pattern because in such parts of the image, R_g is negligible and the R_{sky} contribution can be kept very small if a clear sky area is properly chosen.

Defining B as the value of R relative to R_A and assuming that the atmospheric transmittance T is constant through the area of study, the ratio of the values of B in two arbitrary points of the glitter pattern is

$$\frac{B}{B'} = \frac{R_g}{R_g'} = A \exp\left[-\frac{1}{\sigma^2}(\tan^2 \theta_n - \tan^2 \theta_n')\right] \quad (11)$$

where the prime denotes one of the points and

$$A = \frac{r(\omega) \cos \theta_0' \cos \theta' \cos^4 \theta_n'}{r(\omega') \cos \theta_0 \cos \theta \cos^4 \theta_n} \quad (12)$$

Combining (11) and (2), we obtain

$$V = \frac{1}{512 \times 10^{-5}}\left[\frac{(\tan^2 \theta_n' - \tan^2 \theta_n)}{\ln (B/AB')} - 3 \times 10^{-3}\right] \quad (13)$$

which relates the wind speed V in meters per second to the broadening of the glitter pattern, defined by the difference between θ_n and θ_n'.

Satellite measurements of radiance are given in digitized form as integer counts N linearly related to the reflectance [*Lauritson et al.*, 1979]. B can thus be replaced by N in (13) without precise knowledge of the relationship between the radiance and the digital count. Equation (13) then becomes

$$V = \frac{1}{512 \times 10^{-5}}\left[\frac{(\tan^2 \theta_n' - \tan^2 \theta_n)}{\ln (N - N_A)/[A(N' - N_A)]} - 3 \times 10^{-3}\right] \quad (14)$$

where N_A is the smallest count one can find in the image.

Then using (5), (6), (12), and (14), wind speed can be easily deduced from the positions of the sun and of the satellite and from the digital counts for two arbitrary points of the glitter pattern. The wind speed can be derived at any number of locations, giving the knowledge of the wind magnitude field at synoptic scales.

In following sections, results of wind speed estimations from TIROS-N imagery are presented.

5. Satellite Data

Glitter observations are provided by the TIROS-N satellite series imagery. These satellites are near-polar and sun-synchronous orbiting. Altitude is about 900 km, and the ground swath is about 3000 km. The sensors of the AVHRR are in the visible, the near infrared, and the thermal infrared region [*Schwalb*, 1978]. The data were kindly provided by Centre de Météorologie Spatiale in Lannion (France) in the high-resolution picture transmission mode.

Our purpose is to test a worldwide-working method. As the automatic picture transmission (APT) stations are widely used throughout the world, we degrade the data by selecting only one point in four in both directions on each image in order to have a product similar to those received by APT stations.

Following the conclusions of section 3, only the channel 2 (0.7–1.1 μm) data are used. The 1024 values of the original digital coding are transformed into a 256-value coding by dividing the digital counts by 4.

Satellite data computer compatible tapes are processed at Ecole des Mines, and images are printed on an electrostatic printer with enhancement of the glitter pattern. Such images are shown in Figures 2 and 3. Glitter patterns are clearly visible. Note that more than one pattern can be visible on images and also that except for the brightest areas, the isophotes run nearly parallel to the satellite track, in close agreement with the model of *Cox and Munk* [1954]. Thus one can see that wind speed can be estimated all along the satellite orbit at a considerable number of locations.

On each image, wind magnitude can be estimated within the glitter pattern at grid locations, the sizes of the rectangular mesh being 1 km in the along-track direction and 10 to 60 km in the cross-track direction, depending on the wind speed. Such a resolution allows the study of the wind magnitude mesoscale variability, and this subject will be treated in a forthcoming paper.

The aim of this paper is to prove the efficiency of such a method, showing the close agreement between the wind mag-

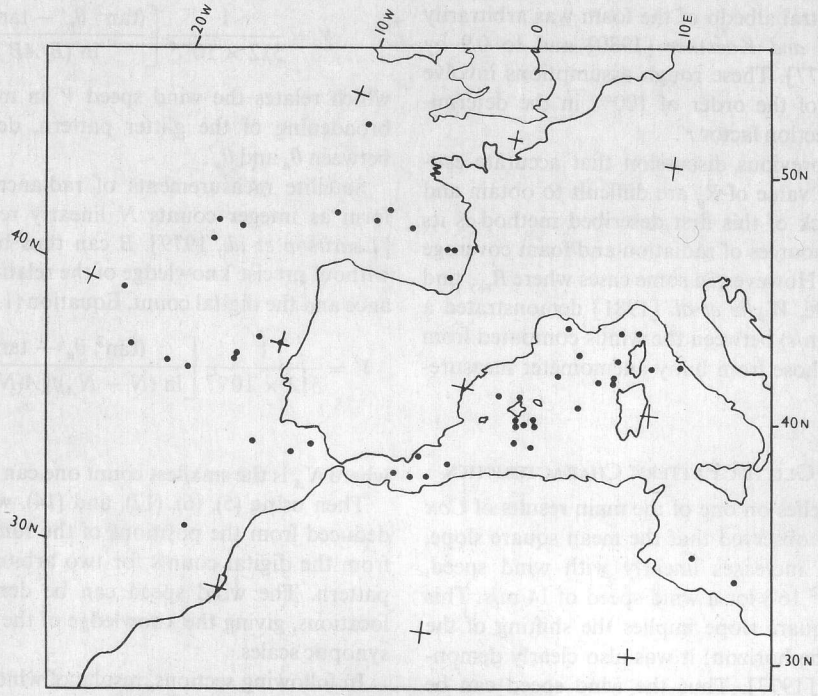

Fig. 4. Map showing the locations of the 51 cores of glitter pattern observed in the AVHRR imagery.

nitude derived from the glitter pattern geometric characteristics and the magnitude derived from the isobaric charts. Consequently, a great number of images have been processed for various geographical locations of the glitter pattern core and for various sun and satellite positions.

For processing simplicity, within each glitter pattern, only two points are arbitrarily chosen for which the positions of the sun and the satellite are computed. Their values are the result of local averaging to avoid radiometric noise, variations in satellite attitude, and small-scale wind variability. Typical values of the digital counts range from 11 to 40 and correspond to reflectances ranging from 0 to 4% [*Lauritson et al.*, 1979].

Then using (5), (6), (12), and (14), the wind speed is computed. For example, on July 23, 1979 (Figure 2), a wind speed of 6.5 m/s has been computed for location 39°N; 4°E (south Balearic Islands), and the direction is predicted to be NE-SW while for location 45°N; 2°W (Bay of Biscay) a wind speed of 3 m/s has been computed, and a NW-SE direction predicted. From Figure 3, taken on July 17, 1980, a wind speed of 7.5 m/s and a NE-SW direction were predicted for location 39°N; 12°W (off Portugal) while a wind speed of 3 m/s and a NE-SW direction were predicted for location 44°N; 15°W (off northern Portugal).

One must take care when looking at the glitter patterns on the edge of the images because at such high viewing angles those bright areas are often caused by sunlight reflection within the atmosphere and applying the method to such glitters gives erratic values of V. To determine if a glitter pattern originates from the sea surface or within the atmosphere, one can refer to the tables of typical reflectance computed by *Wald and Monget* [1982] as a function of the reflection geometry.

6. Wind Data

In order to test the method, the computed wind speeds were compared to the wind speed observations available through the World Meteorological Net.

For the French coastal zones, wind data were provided by direct measurements. In the other cases, wind is estimated from synoptic charts of the earth surface edited by the French Meteorological Office (charts at 600 and 1800 UT) and by the German Meteorological Office (charts at 000 and 1200 UT).

Capitalizing on the small difference (10%) between the actual and the geostrophic wind speeds for mid-latitude synoptic systems [*Holton*, 1972], it can be assumed for this study that the chart-derived winds represent the mesoscale actual winds.

The French Meteorological Office recommends a reduction of the chart-deduced wind by 30% to account for the sea surface roughness [*Direction de la Météorologie Nationale*, 1972]. However, as the Mediterranean Sea reduced winds are always smaller than the winds recorded in coastal meteorological stations by the same amount, it was decided not to reduce the chart-derived winds for the Mediterranean Sea. The cause of this observation is likely linked to the presence of major islands and fetch-limited areas in the sea but is beyond our present scope.

7. Results

Fifty-one glitter patterns were observed from satellite imagery. Their locations are shown in Figure 4 and also reported in Table 1. Twenty-three patterns were located in the Atlantic Ocean, and 28 in the western Mediterranean Sea. From these patterns, 58 wind speeds were estimated: 26 for the Atlantic Ocean and 32 for the Mediterranean Sea. No difference in the results between these two areas can be found.

The estimated speeds range from 2.3 to 8.5 m/s for the Atlantic Ocean and from 0 to 17 m/s for the Mediterranean Sea.

The correlation coefficient between the computed and the chart-derived wind speeds is equal to 0.98 and ensures the linearity of the relationship between the two data sets (Figure 5). When fitted by a least squares method, this relation is written:

$$V_{\text{glitter}} = 1.007 V_{\text{obs}} - 0.174 \qquad (15)$$

where V is in meters per second. The standard deviation from the relationship is equal to 0.5 m/s. Thus this relationship shows very close agreement between the two data sets and clearly demonstrates the success of this method.

TABLE 1. Parameters of Each Glitter Pattern Observation

Date	Satellite	Orbit	Latitude	Longitude	UT	ϕ_0, deg	θ_0, deg	ϕ, deg	θ, deg
April 7, 1979	TN	2484	42°N	6°E	1427	238	52	75	26
May 11, 1979	TN	2963	42°N	10°E	1333	241	38	74	22
May 11, 1979	TN	2964	40°N	18°W	1514	240	35	75	29
May 11, 1979	TN	2964	32°N	12°W	1514	256	37	78	25
May 13, 1979	TN	2992	40°N	11°W	1453	242	36	75	25
June 16, 1979	TN	3471	45°N	2°W	1357	233	31	72	40
July 13, 1979	TN	3852	40°N	2°E	1417	249	35	75	19
July 13, 1979	TN	3852	45°N	9°W	1417	228	30	75	41
July 15, 1979	TN	3880	41°N	7°E	1353	247	34	76	18
July 18, 1979	TN	3923	43°N	15°W	1503	237	3	75	26
July 23, 1979	TN	3993	39°N	4°E	1410	248	36	75	19
July 23, 1979	TN	3993	45°N	2°W	1410	223	35	72	32
Aug. 16, 1979	TN	4332	39°N	12°W	1456	236	37	75	27
Aug. 16, 1979	TN	4333	38°N	14°W	1456	235	35	75	35
Sept. 7, 1979	TN	4642	40°N	10°W	1424	222	41	75	45
March 30, 1980	TN	7534	39°N	4°E	1402	229	46	75	37
April 3, 1980	N6	3990	42°N	8°E	0807	115	59	285	40
April 4, 1980	N6	4004	42°N	12°E	0745	114	60	285	37
April 5, 1980	N6	4019	49°N	9°W	0903	116	63	292	26
April 21, 1980	N6	4246	43°N	8°E	0813	112	52	286	43
April 22, 1980	N6	4260	43°N	9°E	0751	109	5	286	31
April 26, 1980	N6	4317	41°N	5°E	0804	104	53	285	30
April 28, 1980	N6	4345	34°N	13°E	0725	97	54	283	33
May 3, 1980	N6	4416	33°N	15°E	0715	95	54	283	32
May 19, 1980	TN	8240	46°N	6°W	1450	240	39	72	22
May 20, 1980	TN	8254	36°N	1°E	1435	257	39	77	25
June 2, 1980	N6	4843	40°N	6°E	0753	94	50	285	17
June 11, 1980	N6	4971	41°N	8°E	0755	95	48	286	32
June 29, 1980	N6	5227	43°N	5°E	0759	98	50	287	22
June 29, 1980	N6	5227	38°N	4°E	0759	93	50	284	26
July 4, 1980	N6	5298	41°N	8°E	0750	949	49	285	28
July 17, 1980	TN	9073	39°N	12°W	1524	252	37	75	27
July 17, 1980	TN	9073	44°N	15°W	1525	243	37	73	28
July 21, 1980	TN	9129	44°N	2°W	1438	251	42	72	26
July 21, 1980	TN	9129	37°N	0°E	1438	260	42	76	25
July 22, 1980	TN	9143	39°N	3°E	1427	254	38	76	28
July 23, 1980	TN	9157	39°N	3°E	1416	250	36	76	32
Aug. 5, 1980	TN	9341	36°N	2°W	1509	256	43	76	05
								256	04
Aug. 6, 1980	TN	9355	45°N	5°W	1458	221	42	72	25
Aug. 6, 1980	TN	9355	36°N	3°W	1458	253	40	76	21
Aug. 9, 1980	TN	9397	39°N	4°E	1424	247	41	75	24
Aug. 10, 1980	TN	9411	40°N	3°E	1413	241	39	75	29
Aug. 31, 1980	N6	6123	38°N	3°E	0811	106	57	284	38
Sept. 18, 1980	TN	9962	36°N	8°W	1512	238	51	74	34
Sept. 18, 1980	TN	9962	37°N	9°W	1512	238	53	74	42
Aug. 2, 1981	N7	0567	38°N	15°W	1440	232	29	76	20
Aug. 2, 1981	N7	0567	38°N	17°W	1440	229	27	76	28
Aug. 3, 1981	N7	0581	44°N	14°W	1429	222	32	72	20
Aug. 3, 1981	N7	0581	36°N	10°W	1429	239	29	77	14
Aug. 15, 1981	N7	0750	37°N	2°W	1354	234	34	76	26
Aug. 15, 1981	N7	0750	45°N	6°W	1354	220	37	72	19

The TIROS-N satellite is abbreviated TN, NOAA6 is abbreviated N6, and NOAA7 is abbreviated N7.

However, this method does not give the direction of wind in all cases. Because the crosswind and upwind rms are different (equation (2)), the wave slope distribution displays anisotropy. This can be seen in Figures 2 and 3, where the brightest isophotes are elliptic with the great axis along the direction of wind. Then wind direction can be inferred from the orientation of the core of the glitter pattern with a remaining ambiguity of 180°. In some cases, however, the pattern core is hidden by clouds, or the orientation of the central isophotes is not clearly visible, and no axis can be estimated.

As a general rule, the orientation of the central part becomes more and more defined as the wind speed decreases. However, the relationship is rather complex and is strongly related to the gustiness of the wind, as previously shown by *Cox and Munk* [1954]. Steady winds would lead to small values in σ_c^2/σ_u^2 and the corresponding glitter patterns would show anisotropy, whereas gusty winds would increase this ratio to somewhere near unity.

From the 51 observational cases, 28 wind directions (15 for the Atlantic Ocean and 13 for the Mediterranean Sea) were predicted with an accuracy of 20° and an ambiguity of 180°.

8. Discussion

The wind speeds computed by this method range from 0 to 17 m/s or more, but directions are not defined in all cases.

Change in the sun azimuth during the year is a limitation of this method. In winter the difference between the sun and satellite azimuths reaches its minimum value and ranges for the

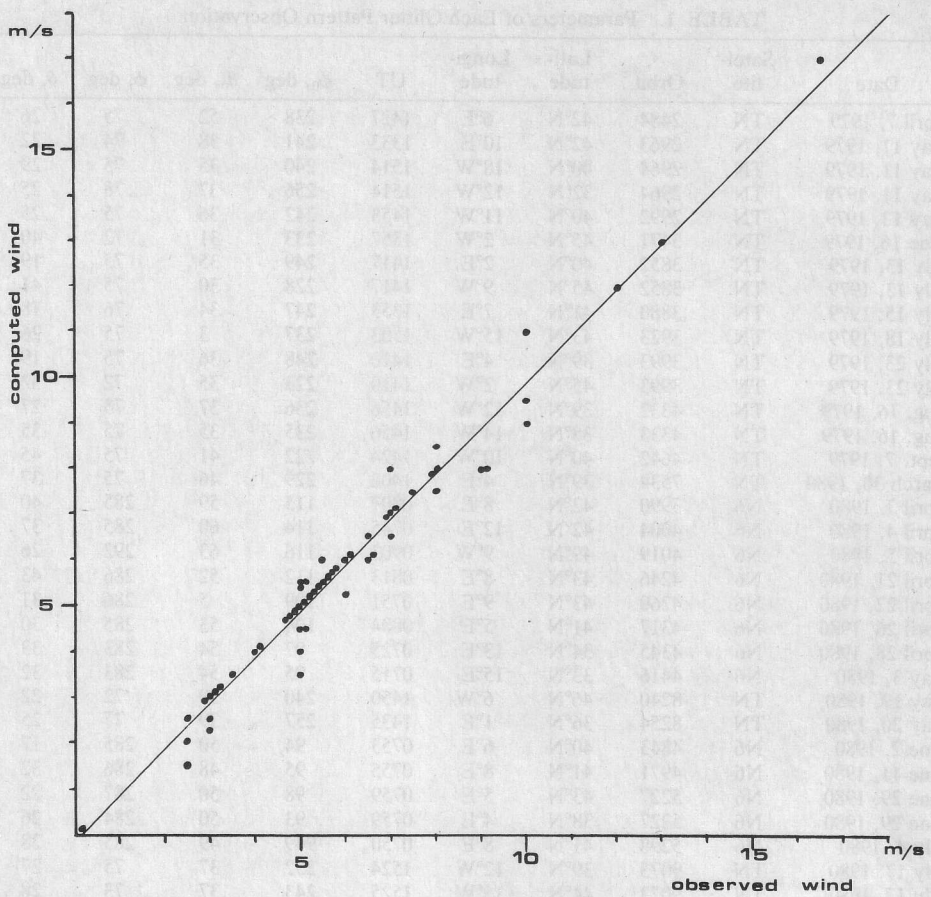

Fig. 5. Computed winds versus chart-derived winds.

mid-latitudes from 90° to 110° depending on the time of the day. In these cases and according to the results of *Wald and Monget* [1982], only a near-vertical sighting and small sun zenith angle will give a well-pronounced glitter pattern. As these conditions are not encountered in mid-latitudes, no winter imagery was used in this study.

LaViolette et al. [1980] discussed the complex features apparent in the sun glint area. Phenomena other than winds can affect the brightness of the sea surface. These authors report that the relative velocity between a uniform wind and the sea surface will be changed by surface currents which would result in noticeable roughness variations under very low wind conditions. They outlined also that the wind stress can be markedly dependent on the degree of stability of the atmospheric boundary layer, and they suggested that roughness variations across the thermal front may be interpreted as a stability modification. Finally, strong current systems affect the direction and shapes of waves, resulting in roughness variations.

These various interactions would cause problems in the extraction of surface winds, and they must be carefully evaluated. For instance, in western regions of major ocean basins the strong and variable currents would render this technique difficult to use.

Except for the above discussed limitations, cloud coverage or absence of sunlight, it is possible to estimate wind over all the world ocean except for high latitudes.

TIROS-N series satellites are sun-synchronous orbiting. Each orbit is about 2300 km westward from the previous one when crossing the equator while the swath is about 3000 km wide. Because these satellites are sun-synchronous, the geometrical conditions for seeing glitter do not vary, and the glitter pattern will be about 2300 km westward from the previous one observed at the equator and less for mid-latitudes. As the glitter pattern is visible along the whole track (except for high latitudes), one can expect to estimate wind by this method in any area.

9. CONCLUSION

A simple method has been presented for deriving wind from space observations of the sun glitter. Only APT station data are required.

This method gives good results for wind speeds but suffers some restrictions: direction can be predicted with an ambiguity of 180° only if the wind is steady; sunlight and cloud-free coverage are needed.

When looking at the results, this method can hardly compare to the scatterometer of SEASAT, which was an all-weather sensor and gave estimates of wind speeds ranging from 0 to 24 m/s with a rms of 2 m/s and a wind direction modulo 180° with a rms of 20° [*Fernandez-Partagas and Estoque*, 1981; *Wylie et al.*, 1981]. It compares fairly well to the sensor scanning multichannel microwave radiometer (SMMR) aboard Nimbus 7, which is also an all-weather sensor and gives wind speeds ranging from 0 to 24 m/s with a rms of 2.5 m/s but cannot give direction. However, the processing of SEASAT scatterometer data or SMMR data is more complex and a greater consumer of computer time than this simple method, with the result that the main advantages of our method are simplicity and scope of possible applications.

Observations are presented in this paper from TIROS-N series satellites, but other spacecraft acquiring the same kind of

data such as METEOSAT, GOES, AEM-1, Nimbus 7, and the Meteor series satellites could also be used in the same fashion.

The wind magnitude can be derived at any number of locations, which is useful in remote areas of the ocean where surface pressure charts are not always available. In the authors' opinion, this technique has promise for routine meteorological analysis.

As an example, during the next U.S. experiment SEQUAL and the French one FOCAL, using this method with METEOSAT and GOES observations could prove to be of great interest in studies of large-scale wind effects on the ocean dynamics in the tropical zone.

Acknowledgments. The authors thank P. Delecluse, C. Millot, and B. Wannamaker for their helpful discussions and suggestions. They are grateful to the referees for their criticisms about this paper.

REFERENCES

Cox, C., and W. Munk, Statistics of the sea-surface derived from sun glitter, *J. Mar. Res.*, *13*(2), 198–227, 1954.

Cox, C., and W. Munk, Some problems in optical oceanography, *J. Mar. Res.*, *14*(1), 63–78, 1955.

Direction de la Météorologie Nationale, Bulletin quotidien de renseignements de la météorologie nationale: Notice explicative, p. 3, Ministère des Transports, Paris, 1972.

Fernandez-Partagas, J. J., and M. A. Estoque, Analysis of SEASAT wind observations over the Indian Ocean, *Tellus*, *33*, 463–475, 1981.

Gordon, H. R., and M. M. Jacobs, Albedo of the ocean-atmosphere system: Influence of sea foam, *Appl. Opt.*, *16*(8), 2257–2260, 1977.

Holton, J. R., *An Introduction to Dynamic Meteorology*, pp. 44–45, Academic, New York, 1972.

Ivanoff, A., *Introduction à l'Océanographie*, vol. 2, pp. 24–35, Vuibert, Paris, 1975.

Jerlov, N. G., *Marine Optics*, *Elsevier Oceanogr. Ser.*, vol. 14, p. 130, Elsevier Sci., New York, 1976.

Lauritson, L., G. J. Nelson, and F. W. Porto, Data extraction and calibration of TIROS-N NOAA radiometers, *NOAA Tech. Memo. NESS 107*, p. 46, 1979.

LaViolette, P. E., S. Petherych, and J. F. R. Gower, Oceanographic implications of features in NOAA satellite visible imagery, *Boundary Layer Meteorol.*, *18*(2), 159–176, 1980.

Levanon, N., Determination of the sea surface slope distribution and wind velocity using sun glitter viewed from a synchronous satellite, *J. Phys. Oceanogr.*, *10*, 214–220, 1971.

McClain, E. P., and A. E. Strong, On anomalous dark patches in satellite-viewed sunglint areas, *Mon. Weather Rev.*, *97*(12), 875–884, 1969.

Monahan, E. C., and I. O. Muircheartaigh, Optimal power-law description of oceanic whitecap coverage dependence on wind speed, *J. Phys. Oceanogr.*, *10*, 2094–2099, 1980.

Plass, G. N., G. W. Kattawar, and J. A. Guinn, Jr., Radiative transfer in the earth's atmosphere and ocean: Influence of ocean waves, *Appl. Opt.*, *14*(8), 1924–1936, 1975.

Plass, G. N., G. W. Kattawar, and J. A. Guinn, Jr., Isophotes of sunlight glitter on a wind-ruffled sea, *Appl. Opt.*, *16*(3), 643–653, 1977.

Quenzel, H., and M. Kaestner, Optical properties of the atmosphere: Calculated variability and application to satellite remote sensing of phytoplankton, *Appl. Opt.*, *19*(8), 1338–1344, 1980.

Ross, D. B., and V. J. Cardone, Observations of oceanic whitecaps and their relation to remote measurements of surface wind speed, *J. Geophys. Res.*, *79*(3), 444–452, 1974.

Ross, D. B., V. J. Cardone, and J. W. Conway, Jr., Laser and microwave observations of sea-surface condition for fetch-limited 17 to 25 m/s winds, *IEEE Trans. Geosci. Electron.*, *8*(4), 326–336, 1970.

Rozenberg, G. V., and Yu.-A. R. Mullamaa, Some possibilities of determining wind over an ocean surface using observations from artificial earth satellites, *Izv. Acad. Sci. USSR Atmos. Oceanic Phys.*, Engl. Transl., *1*(3), 282–290, 1965.

Schwalb, A., The TIROS-N/NOAA A-G satellite series, *NOAA Tech. Memo. NESS 95*, 1978.

Soules, S. D., Sun glitter viewed from space, *Deep Sea Res.*, *17*, 191–195, 1970.

Strong, A. E., and I. S. Ruff, Utilizing satellite-observed solar reflections from the sea-surface as an indicator of surface wind speeds, *Remote Sens. Environ.*, *1*, 181–185, 1970.

Viollier, M., D. Tanre, and P. Y. Deschamps, An algorithm for remote sensing of water color from space, *Boundary Layer Meteorol.*, *18*, 247–267, 1980.

Wald, L., and J. M. Monget, Remote sensing of the sea-state using the 0.8–1.1 microns spectral band, *Int. J. Remote Sens.*, in press, 1982.

Webber, D. S., Surface winds from sun glitter measurements from a space craft, *Proc. Soc. Photo Opt. Instrum. Eng.*, *27*, 93–100, 1971.

Wylie, D. P., B. B. Hinton, and K. M. Millet, A comparison of three satellite-based methods for estimating surface winds over oceans, *J. Appl. Meteorol.*, *20*, 439–449, 1981.

(Received July 26, 1982;
revised November 4, 1982;
accepted November 4, 1982.)